An Active Elastic Support/Dry Friction Damper: New Modeling and Analysis for Vibration Control of Rotor Systems

Siji Wang(✉), Mingfu Liao, Mingbo Song, and Yingge Xu

School of Power and Energy, Northwestern Polytechnical University, Xi'an 710072, China
sjwang@nwpu.edu.cn

Abstract. This article introduces a new type of active damper—elastic support/dry friction damper (ESDFD) for vibration control of rotor systems and its performances. The basic operation principle of ESDFD in rotor system was introduced. In particular, a two-dimensional friction model-ball/plate model was proposed, by which a dynamic model of rotor systems with ESDFD was established and verified. The damping performance of the ESDFD has been studied numerically. The simulation results show that the damping performance of ESDFD is closely related to the characteristics of the rotor's mode. For obtaining the damper's best performance, the damper should be located at the elastic support in which the vibration energy is concentrated. And the damper not only provides external damping to the rotor system, but also increases extra stiffness into the rotor system. The stiffness of the stationary disk and the tangential contact stiffness of the contact interface are connected in series between the moving disk and the mounting base of the stationary disk. The larger of this combined stiffness, the better of the damper's damping performance. The application of ESDFD to the vibration suppression of a rotor system is investigated experimentally. A switch control scheme for the damper is introduced; the effectiveness and control characteristics with control scheme for attenuating the vibration of rotor systems are experimentally investigated.

Keywords: Active elastic support/dry friction damper
Ball/plate model of friction · P control · Rotor systems

1 Introduction

Traditional damper of rotor systems in aero engines, such as squeeze film dampers, is passive device because it cannot adjust its damping ratio in response to changes of unbalance response in the rotor system operating conditions. To overcome this deficiency, active dampers have been suggested as a means of control unbalance response of the rotating machine. The ESDFD is a new type of damper for active vibration

The present work is supported by the National Natural Science Foundation of China (Project No: 51405393).

K. L. Cavalca and H. I. Weber (Eds.): IFToMM 2018, MMS 62, pp. 19–33, 2019.
https://doi.org/10.1007/978-3-319-99270-9_2

control of rotor systems in aero engines [1]. It can active control unbalance response of the rotor system through active damping and stiffness. A magnetic bearing is one of promising type of active bearings and has been the subject of extensive research. It is well suited for high-speed rotating machine because of its non-contact nature and its unique ability to suspend loads with no friction. However, because of its low load-carrying capacity and heavy weight, relative to a mechanical bearing, a magnetic bearing is not suitable for vibration control in aero engines.

The ESDFD is one promising damper candidate for active vibration control in aero engines. It has been proven theoretically and experimentally that the damper can significantly attenuate the unbalance response of a rotor system. There are several older applications of such systems, Fan et al. [2] proposed that friction damping could be applied in rotor system. Wang et al. [3–5], designed an active elastic support/dry friction damper using an electromagnetic actuator or piezoelectric ceramic actuator, which can conveniently be actively controlled by adjusting the control voltage of the electromagnet or piezoelectric ceramic actuator. Usually, dry friction is disadvantageous in mechanical systems, such as in rubbing faults of rotor systems [6–8]. However, as external damping, dry friction has been widely used to increase the stability of mechanical systems, such as the dry friction damping blade of aero engines and turbines [9–15]. Figure 1 shows the operation principles of a rotor with ESDFDs. The rotor is supported by two elastic supports, and at the end cross section of each one, the dry friction damper is affixed. Each damper consists of three key components: the elastic support, the friction pairs (stationary disk and moving disk) and the actuator. The elastic supports redistribute the strain energy of the whole rotor-support system and concentrate the vibration, which is then dissipated by the dry friction between the friction pairs. The moving disk, which is fixed to the end cross section of the elastic support, is connected to the bearing outer ring and vibrates with the elastic support but does not rotate with the rotor. The stationary disk is fixed to the casing and can be moved in the axial direction by the actuator. The frictional force between the two disks can be changed by adjusting the pressure force from the actuator.

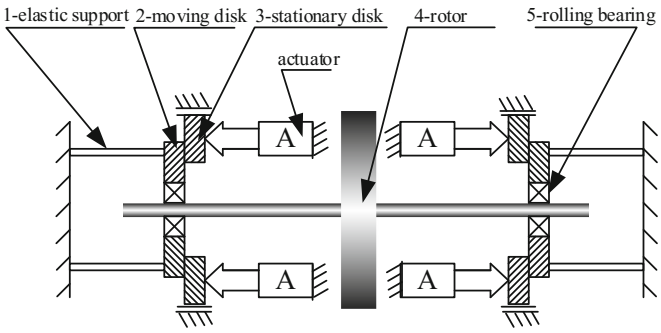

Fig. 1. The operation principles of the ESDFD

The work to propose the mechanism model of the ESDFD was Fan et al. [1, 2], in which the rotor was simplified to a single degree of freedom system, and dry friction model was the classic one-dimensional hysteretic. The classic one-dimensional hysteretic dry friction model was just for illustrating the friction damping mechanism of the dry friction damper, and was insufficient for the damper designing of rotor systems. There are two reasons. The first one is the axial location of the damper influences the damping performance of the elastic support/dry friction damper, which cannot be considered in the previous work; the second one is the relative motion between the friction pair is a two-dimensional motion, which is considered as one-dimensionally in the previous work.

This work departs from the existing hysteretic dry friction model, a two-dimensional friction model-ball/plate model is proposed by which dynamic model of a rotor system with ESDFDs was established and verified. According to the characteristics of the ESDFD, A control scheme was introduced; the effectiveness and control characteristics for the vibration control of the rotor system were experimentally investigated.

2 Damper and Rotor System Model

2.1 Two-Dimensional Friction and Ball/Plate Model

A two-dimensional friction model-ball/plate model (shown in Fig. 2) is proposed. The model was developed from the hysteretic dry friction model. As shown in Fig. 2, the stationary disk is represented by a rectangle and remains at rest. The moving disk consists of a ball and a plate. The plate (without considering its mass) represents the contact interface between the moving disk and the stationary disk, and the ball represents the moving disk. The ball and the plate are connected with ideal springs and linear damping in two directions. The ideal springs represent the tangential contact stiffness of the contact interface. The displacement between the ball and the plate represents the microscopic sliding in the state of stick. So if the applied force on the ball is greater than maximum stick, the ball will touch the edge of the plate, and the plate will begin to move.

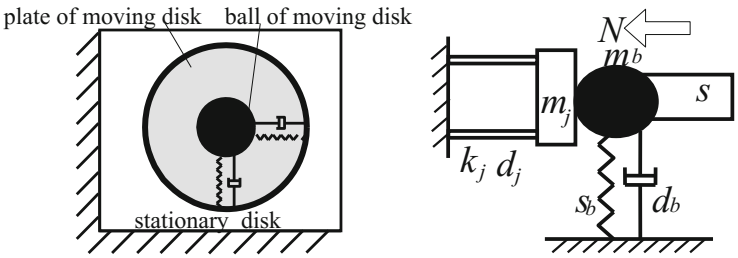

Fig. 2. Two-dimensional friction and ball/plate model

The ball/plate dry friction model is actually a type of two-dimensional hysteretic dry friction model. The frictional force between the stationary disk and the plate is Coulomb's friction force. The frictional force at any time depends on the motion state of the plate and the applied force with which the ball acts on the plate.

Without considering the mass of the plate, the resultant force acting on the plate will be 0 at any time. When the plate is stationary relative to the stationary disk, namely the friction pair is in the state of stick, the frictional force acting on the plate is

$$F_f = -[k(r_1 - r_2) + d(\dot{r}_1 - 0)] < \mu N \tag{1}$$

If $|k(r_1 - r_2) + d(\dot{r}_1 - 0)| \geq \mu N$, the plate will not remain stationary relative to the stationary disk, namely the friction pairs is in the state of kinetic friction, and the frictional force acting on the plate is

$$F_f = -\frac{\dot{r}_2 - \dot{r}_j}{|\dot{r}_2 - \dot{r}_j|}\mu N \tag{2}$$

where $r_1 = x_1 + iy_1$ is the displacement of the ball; $r_2 = x_2 + iy_2$ is the displacement of the plate; $r_j = x_j + iy_j$ is the displacement of the stationary disk, its value is 0 when the stationary disk remains at rest; k is the stiffness coefficient between the ball and the plate; d is the damping coefficient between the ball and the plate; μ is the friction coefficient; and N is the pressure force.

2.2 Dynamics Model with the Rotor Systems

As shown in Fig. 3 is s single-disk flexible rotor with ESDFDs. The system consists of two parts: a rotor and two ESDFDs (in the dashed boxes). The rotor is a single offset disk with a flexible shaft that is supported by two elastic supports at both ends. The two ESDFDs can be set up at each elastic support, shown in the dashed boxes of Fig. 3.

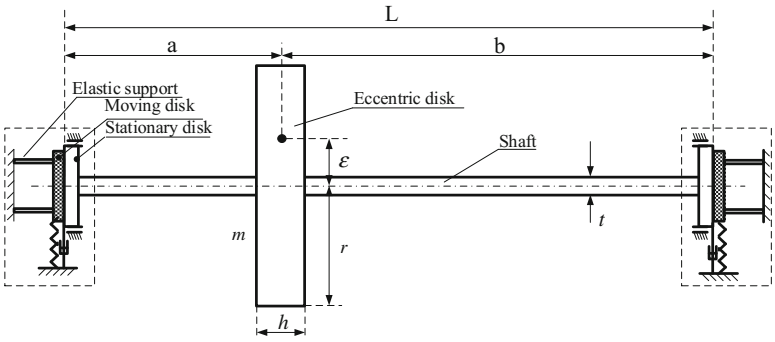

Fig. 3. A single-disk flexible rotor with ESDFDs

For the rotor disk, four coordinates are required to describe its motion. Two of them (x, y) describe its two-dimensional translation; the other two (φ_x, φ_y) describe its two-dimensional swing. For the left friction pair, six coordinates are required to describe the two-dimensional motion of the moving disk (the ball and the plate) and the stationary disk: x_{b1} and y_{b1} describe the motion of the ball; x_{d1} and y_{d1} describe the motion of the plate; and x_{j1} and y_{j1} describe the motion of the stationary disk. In the same way, another 6 coordinates describe the motion of the right friction pair. They are x_{b2}, y_{b2}, x_{d2}, y_{d2}, x_{j2}, y_{j2}. So in total, the whole rotor system is a system with 16 degrees of freedom (16-DOF system).

By means of Euler's laws of motion, the motion equations of the rotor disk, moving disk and stationary disk can be obtained as follows.

The rotor disk:

$$m\ddot{\mathbf{r}} + s_{11}\mathbf{r} - is_{12}\boldsymbol{\varphi} - (\frac{L-a}{L}s_{11} + \frac{1}{L}s_{12})\mathbf{r_{b1}} - (\frac{a}{L}s_{11} - \frac{1}{L}s_{12})\mathbf{r_{b2}} = m\varepsilon\Omega^2 e^{i\Omega t} \quad (3)$$

$$J_d\ddot{\boldsymbol{\varphi}} - iJ_p\Omega\dot{\boldsymbol{\varphi}} + is_{21}\mathbf{r} + s_{22}\boldsymbol{\varphi} - i(\frac{L-a}{L}s_{21} + \frac{1}{L}s_{22})\mathbf{r_{b1}} - i(\frac{a}{L}s_{21} - \frac{1}{L}s_{22})\mathbf{r_{b2}} = 0 \quad (4)$$

The moving disk (the ball in the ball/plate model):

$$m_{b1}\ddot{\mathbf{r}}_{\mathbf{b1}} + (d_{b1} + d)\dot{\mathbf{r}}_{\mathbf{b1}} + A_1\mathbf{r} + A_2\boldsymbol{\varphi} + A_3\mathbf{r_{b1}} + A_4\mathbf{r_{b2}} = k\mathbf{r_{d1}} + d\dot{\mathbf{r}}_{\mathbf{d1}} \quad (5)$$

where
$$\begin{cases} A_1 = -(\frac{L-a}{L}s_{11} + \frac{1}{L}s_{21}) \\ A_2 = i(\frac{L-a}{L}s_{12} + \frac{1}{L}s_{22}) \\ A_3 = (\frac{L-a}{L})^2 s_{11} + \frac{L-a}{L^2}s_{21} + \frac{L-a}{L^2}s_{12} + \frac{1}{L^2}s_{22} + (s_{b1} + k) \\ A_4 = \frac{(L-a)a}{L^2}s_{11} + \frac{a}{L^2}s_{21} - \frac{L-a}{L^2}s_{12} - \frac{1}{L^2}s_{22} \end{cases}$$

$$m_{b2}\ddot{\mathbf{r}}_{\mathbf{b2}} + (d_{b2} + d)\dot{\mathbf{r}}_{\mathbf{b2}} + B_1\mathbf{r} + B_2\boldsymbol{\varphi} + B_3\mathbf{r_{b1}} + B_4\mathbf{r_{b2}} = k\mathbf{r_{d2}} + d\dot{\mathbf{r}}_{\mathbf{d2}} \quad (6)$$

where
$$\begin{cases} B_1 = -(\frac{a}{L}s_{11} - \frac{1}{L}s_{21}) \\ B_2 = i(\frac{a}{L}s_{12} - \frac{1}{L}s_{22}) \\ B_3 = \frac{(L-a)a}{L^2}s_{11} - \frac{L-a}{L^2}s_{21} + \frac{a}{L^2}s_{12} - \frac{1}{L^2}s_{22} \\ B_4 = (\frac{a}{L})^2 s_{11} - \frac{a}{L^2}s_{21} - \frac{a}{L^2}s_{12} + \frac{1}{L^2}s_{22} + (s_{b2} + k) \end{cases}$$

The stationary disk:

$$m_{j1}\ddot{\mathbf{r}}_{\mathbf{j1}} + d_{j1}\dot{\mathbf{r}}_{\mathbf{j1}} - d\dot{\mathbf{r}}_{\mathbf{b1}} - k\mathbf{r_{b1}} + s_{j1}\mathbf{r_{j1}} = -k\mathbf{r_{d1}} - d\dot{\mathbf{r}}_{\mathbf{d1}} \quad (7)$$

$$m_{j2}\ddot{\mathbf{r}}_{\mathbf{j2}} + d_{j2}\dot{\mathbf{r}}_{\mathbf{j2}} - d\dot{\mathbf{r}}_{\mathbf{b2}} - k\mathbf{r_{b2}} + s_{j2}\mathbf{r_{j2}} = -k\mathbf{r_{d2}} - d\dot{\mathbf{r}}_{\mathbf{d2}} \quad (8)$$

The plate of the moving disk (the plate in the ball/plate model):

$$\dot{\mathbf{r}}_{\mathbf{d1}} = \begin{cases} \dot{\mathbf{r}}_{\mathbf{j1}}, & \left|k(\mathbf{r_{b1}} - \mathbf{r_{d1}}) + d(\dot{\mathbf{r}}_{\mathbf{b1}} - \dot{\mathbf{r}}_{\mathbf{j1}})\right| < \mu N_1 \\ \dot{\mathbf{r}}_{\mathbf{b1}} - \left[\frac{\mu N_1}{d}\frac{k(\mathbf{r_{b1}} - \mathbf{r_{d1}}) + d(\dot{\mathbf{r}}_{\mathbf{b1}} - \dot{\mathbf{r}}_{\mathbf{j1}})}{\left|k(\mathbf{r_{b1}} - \mathbf{r_{d1}}) + d(\dot{\mathbf{r}}_{\mathbf{b1}} - \dot{\mathbf{r}}_{\mathbf{j1}})\right|} - \frac{k}{d}(\mathbf{r_{b1}} - \mathbf{r_{d1}})\right], & \left|k(\mathbf{r_{b1}} - \mathbf{r_{d1}}) + d(\dot{\mathbf{r}}_{\mathbf{b1}} - \dot{\mathbf{r}}_{\mathbf{j1}})\right| \geq \mu N_1 \end{cases} \tag{9}$$

$$\dot{\mathbf{r}}_{\mathbf{d2}} = \begin{cases} \dot{\mathbf{r}}_{\mathbf{j2}}, & \left|k(\mathbf{r_{b2}} - \mathbf{r_{d2}}) + d(\dot{\mathbf{r}}_{\mathbf{b2}} - \dot{\mathbf{r}}_{\mathbf{j2}})\right| < \mu N_2 \\ \dot{\mathbf{r}}_{\mathbf{b2}} - \left[\frac{\mu N_2}{d}\frac{k(\mathbf{r_{b2}} - \mathbf{r_{d2}}) + d(\dot{\mathbf{r}}_{\mathbf{b2}} - \dot{\mathbf{r}}_{\mathbf{j2}})}{\left|k(\mathbf{r_{b2}} - \mathbf{r_{d2}}) + d(\dot{\mathbf{r}}_{\mathbf{b2}} - \dot{\mathbf{r}}_{\mathbf{j2}})\right|} - \frac{k}{d}(\mathbf{r_{b2}} - \mathbf{r_{d2}})\right], & \left|k(\mathbf{r_{b2}} - \mathbf{r_{d2}}) + d(\dot{\mathbf{r}}_{\mathbf{b2}} - \dot{\mathbf{r}}_{\mathbf{j2}})\right| \geq \mu N_2 \end{cases} \tag{10}$$

Where $\mathbf{r} = x + iy$ is the displacement of the rotor disk; $\boldsymbol{\varphi} = \varphi_x + i\varphi_y$ is the swing angle of the rotor disk; $\mathbf{r_{b1}} = x_{b1} + iy_{b1}$ is the displacement of the left moving disk; $\mathbf{r_{b2}} = x_{b2} + iy_{b2}$ is the displacement of the right moving disk; $\mathbf{r_{d1}} = x_{d1} + iy_{d1}$ is the displacement of the left plate of the moving disk; $\mathbf{r_{d2}} = x_{d2} + iy_{d2}$ is the displacement of the right plate of the moving disk; $\mathbf{r_{j1}} = x_{j1} + iy_{j1}$ is the displacement of the left stationary disk; $\mathbf{r_{j2}} = x_{j2} + iy_{j2}$ is the displacement of the right stationary disk; m, m_{b1}, m_{b2}, m_{j1}, and m_{j2} respectively represent the masses of the rotor disk, the moving disks and the stationary disks; s_{11}, s_{12}, s_{21} and s_{22} represent the stiffness coefficients of the shaft at the rotor disk, where s_{11} is the displacement stiffness, s_{22} is the angle stiffness, s_{12} and s_{21} are cross stiffness; s_{b1}, s_{b2}, s_{j1}, and s_{j2} respectively represent the stiffness coefficients of the elastic support and the stationary disk; d_{b1}, d_{b2}, d_{j1}, and d_{j2} respectively represent the damping coefficients of the elastic support and the stationary disk; J_p and J_d respectively represent the polar moment of inertia and the moment of inertia about a diameter of the rotor disk; N_1 and N_2 respectively represent the pressing force between the moving disk and stationary disk of the two dampers; k and d are the tangential contact stiffness coefficient and damping coefficient of the contact interface introduced by the ball/plate model; L is the length between the two supports; a is the length between the left support and the rotor disk; ε is the eccentricity of the rotor disk; and Ω is the rotational speed of the rotor.

To solve the equations by numerical methods, the following variables are introduced:

$$\begin{cases} \mathbf{u_1} = \left\{\mathbf{r}, \boldsymbol{\varphi}, \mathbf{r_{b1}}, \mathbf{r_{b2}}, \mathbf{r_{j1}}, \mathbf{r_{j2}}\right\}^T \\ \mathbf{u_2} = \dot{\mathbf{u}}_\mathbf{1} \\ \mathbf{u_3} = \left\{\mathbf{r_{d1}}, \mathbf{r_{d2}}\right\}^T \end{cases} \tag{11}$$

Equations (3)–(10) can be written in the following form:

$$\begin{bmatrix} \mathbf{E} & \mathbf{O} & \mathbf{O} \\ \mathbf{O} & \mathbf{M} & \mathbf{O} \\ \mathbf{O} & \mathbf{O} & \mathbf{E} \end{bmatrix} \begin{Bmatrix} \dot{\mathbf{u}}_\mathbf{1} \\ \dot{\mathbf{u}}_\mathbf{2} \\ \dot{\mathbf{u}}_\mathbf{3} \end{Bmatrix} + \begin{bmatrix} \mathbf{O} & -\mathbf{E} & \mathbf{O} \\ \mathbf{S} & \mathbf{D} & \mathbf{O} \\ \mathbf{O} & \mathbf{O} & \mathbf{O} \end{bmatrix} \begin{Bmatrix} \mathbf{u_1} \\ \mathbf{u_2} \\ \mathbf{u_3} \end{Bmatrix} = \begin{Bmatrix} \mathbf{O} \\ \mathbf{f} \\ \mathbf{f_d} \end{Bmatrix} \tag{12}$$

where

$$[\mathbf{M}]=\begin{bmatrix} m & & & & & & \\ & J_d & & & & & \\ & & m_{b1} & & & & \\ & & & m_{b2} & & & \\ & & & & m_{j1} & & \\ & & & & & m_{j2} \end{bmatrix};$$

$$[\mathbf{S}]=\begin{bmatrix} s_{11} & -is_{12} & -(\frac{L-a}{L}s_{11}+\frac{1}{L}s_{12}) & -(\frac{a}{L}s_{11}-\frac{1}{L}s_{12}) & 0 & 0 \\ is_{21} & s_{22} & -i(\frac{L-a}{L}s_{21}+\frac{1}{L}s_{22}) & -i(\frac{a}{L}s_{21}-\frac{1}{L}s_{22}) & 0 & 0 \\ A_1 & A_2 & A_3 & A_4 & 0 & 0 \\ B_1 & B_2 & B_3 & B_4 & 0 & 0 \\ 0 & 0 & -k & 0 & s_{j1} & 0 \\ 0 & 0 & 0 & -k & 0 & s_{j2} \end{bmatrix};$$

$$[\mathbf{D}]=\begin{bmatrix} 0 & & & & & \\ & -iJ_p\Omega & & & & \\ & & d_{b1}+d & & & \\ & & & d_{b2}+d & & \\ & & -d & & d_{j1} & \\ & & & -d & & d_{j2} \end{bmatrix};$$

$$\{\mathbf{f}\}=\begin{Bmatrix} m\varepsilon\Omega^2 e^{i\Omega t} \\ 0 \\ k\mathbf{r_{d1}}+d\dot{\mathbf{r}}_{\mathbf{d1}} \\ k\mathbf{r_{d2}}+d\dot{\mathbf{r}}_{\mathbf{d2}} \\ -(k\mathbf{r_{d1}}+d\dot{\mathbf{r}}_{\mathbf{d1}}) \\ -(k\mathbf{r_{d2}}+d\dot{\mathbf{r}}_{\mathbf{d2}}) \end{Bmatrix};$$

$$\{\mathbf{f_d}\}=\begin{Bmatrix} \begin{cases} \dot{\mathbf{r}}_{\mathbf{j1}}, & \left|k(\mathbf{r_{b1}}-\mathbf{r_{d1}})+d(\dot{\mathbf{r}}_{\mathbf{b1}}-\dot{\mathbf{r}}_{\mathbf{j1}})\right|<\mu N_1 \\ \dot{\mathbf{r}}_{\mathbf{b1}}-\left[\frac{\mu N_1}{d}\frac{k(\mathbf{r_{b1}}-\mathbf{r_{d1}})+d(\dot{\mathbf{r}}_{\mathbf{b1}}-\dot{\mathbf{r}}_{\mathbf{j1}})}{\left|k(\mathbf{r_{b1}}-\mathbf{r_{d1}})+d(\dot{\mathbf{r}}_{\mathbf{b1}}-\dot{\mathbf{r}}_{\mathbf{j1}})\right|}-\frac{k}{d}(\mathbf{r_{b1}}-\mathbf{r_{d1}})\right], & \left|k(\mathbf{r_{b1}}-\mathbf{r_{d1}})+d(\dot{\mathbf{r}}_{\mathbf{b1}}-\dot{\mathbf{r}}_{\mathbf{j1}})\right|\geq\mu N_1 \end{cases} \\ \begin{cases} \dot{\mathbf{r}}_{\mathbf{j2}}, & \left|k(\mathbf{r_{b2}}-\mathbf{r_{d2}})+d(\dot{\mathbf{r}}_{\mathbf{b2}}-\dot{\mathbf{r}}_{\mathbf{j2}})\right|<\mu N_2 \\ \dot{\mathbf{r}}_{\mathbf{b2}}-\left[\frac{\mu N_2}{d}\frac{k(\mathbf{r_{b2}}-\mathbf{r_{d2}})+d(\dot{\mathbf{r}}_{\mathbf{b2}}-\dot{\mathbf{r}}_{\mathbf{j2}})}{\left|k(\mathbf{r_{b2}}-\mathbf{r_{d2}})+d(\dot{\mathbf{r}}_{\mathbf{b2}}-\dot{\mathbf{r}}_{\mathbf{j2}})\right|}-\frac{k}{d}(\mathbf{r_{b2}}-\mathbf{r_{d2}})\right], & \left|k(\mathbf{r_{b2}}-\mathbf{r_{d2}})+d(\dot{\mathbf{r}}_{\mathbf{b2}}-\dot{\mathbf{r}}_{\mathbf{j2}})\right|\geq\mu N_2 \end{cases} \end{Bmatrix}$$

E is the unit matrix, and **O** is the zero matrix.

Let $\begin{bmatrix} \mathbf{E} & \mathbf{O} & \mathbf{O} \\ \mathbf{O} & \mathbf{M} & \mathbf{O} \\ \mathbf{O} & \mathbf{O} & \mathbf{E} \end{bmatrix}=\mathbf{A}$, $\begin{bmatrix} \mathbf{O} & -\mathbf{E} & \mathbf{O} \\ \mathbf{S} & \mathbf{D} & \mathbf{O} \\ \mathbf{O} & \mathbf{O} & \mathbf{O} \end{bmatrix}=\mathbf{B}$, $\begin{Bmatrix} \mathbf{O} \\ \mathbf{f} \\ \mathbf{f_d} \end{Bmatrix}=\{\mathbf{p}\}$, $\begin{Bmatrix} \mathbf{u_1} \\ \mathbf{u_2} \\ \mathbf{u_3} \end{Bmatrix}=\{\mathbf{u}\}$, then Eq. (12) can be transformed into

$$\{\dot{\mathbf{u}}\}=-\mathbf{A}^{-1}\cdot\mathbf{B}\cdot\{\mathbf{u}\}+\mathbf{A}^{-1}\cdot\{\mathbf{p}\} \tag{13}$$

Equation (13) can be solved by numerical method for ordinary differential equations.

3 Characteristics of a Rotor with ESDFDs

3.1 Rotor Systems with the ESDFDs

Figure 4 shows a rotor system with two ESDFDs. The rotor experimental apparatus consists of a bias disk rotor, two dampers, two self-aligning bearings, a flexible coupling, a motor and two amplifiers for driving the damper.

The amplitude-frequency characteristics of a rotor with ESDFDs under variable pressing force were tested. Two friction pairs were used in the experiments. One was brass/steel, and the other was steel/steel. The test results are shown in Figs. 5a and 6a.

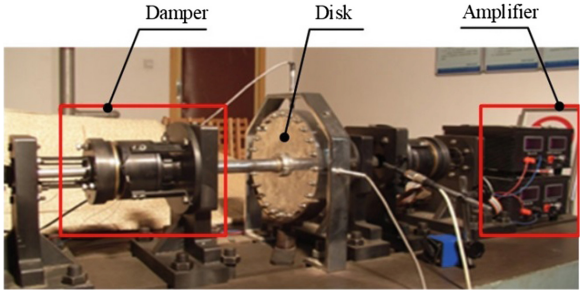

Fig. 4. The rotor system with the ESDFDs

Numerical simulations were carried out using the parameters of the rotor test rig shown in Fig. 4 and the model shown in Fig. 3. The geometrical dimensions of the rotor system are as follows:

L = 700 mm, a = 250 mm, b = 450 mm, t = 28 mm, r = 120 mm, h = 40 mm, and material parameters are $\rho = 7.8 \times 10^3$ kg/m^3, $E = 2.1 \times 10^{11}$ N/m^2.

Based on the geometrical dimensions and material parameters above, the mass, stiffness, moment of inertia, etc., of the rotor can be obtained. In addition, in order to investigate the effect of mode shape on damping effect, m_{b2} is valued much larger than m_{b1} to make the vibration amplitude at the right elastic support higher than left on the second mod. The results are shown in Figs. 5b and 6b.

All of the basic Parameters are listed in Table 1.

Figure 5 shows the amplitude-frequency characteristics when the friction pair is brass/steel, and Fig. 6 shows the amplitude-frequency characteristics when the friction pair is steel/steel. Comparing figure a with figure b in both figures, the calculation results show good agreement with the test results, not only regarding the trend but also the specific values with the damper. Figure 5 shows a significant mismatch for zero N pressure force is that nonlinearity response of rotor systems with a large unbalance.

Table 1. Parameters of the rotor for numerical analysis

Parameters	Values	Parameters	Values
m	15.7 kg	ε	3×10^{-5} m
J_p	0.113 kg m^2	J_d	0.0586 kg m^2
a	250 mm	L	700 mm
s_{11}	1.4251×10^6 N/m	s_{12}	2.1026×10^5 N/m
s_{21}	2.1026×10^5 N/m	s_{22}	1.1827×10^5 N/m
s_{b1}	7.38×10^5 N/m	s_{b2}	7.73×10^5 N/m
d_{b1}	250 Ns/m	d_{b2}	250 Ns/m
m_{b1}	1.6 kg	m_{b2}	12 kg
k	3×10^5 N/m	d	10 Ns/m
m_{j1}	2 kg	m_{j2}	2 kg
s_{j1}	1×10^7 N/m	s_{j2}	1×10^7 N/m
d_{j1}	134 Ns/m	d_{j2}	134 Ns/m
μ (brass/steel)	0.19	μ (steel/steel)	0.1

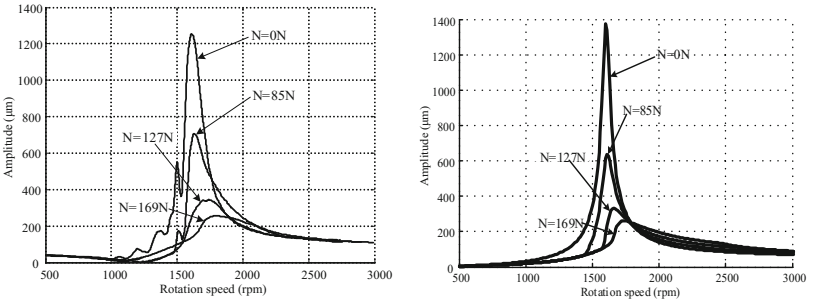

a. Test results b. Calculation results

Fig. 5. Amplitude-frequency characteristics of the rotor, brass/steel

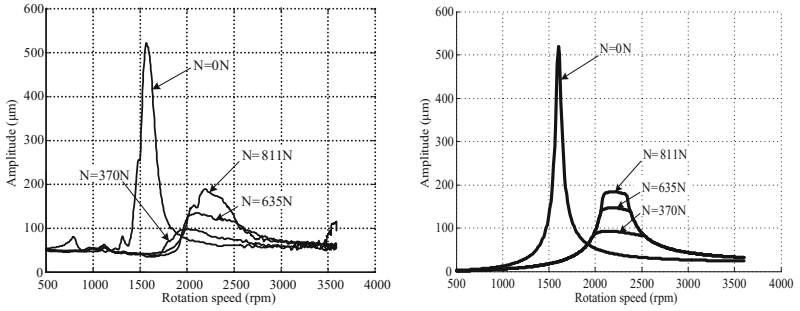

a. Test results b. Calculation results

Fig. 6. Amplitude-frequency characteristics of the rotor, steel/steel

3.2 Characteristics of Damping Performance

Stiffness of the Elastic Support

The critical speed and mode shape can be affected by the elastic support. The performances of the ESDFD with respect to the stiffness of the elastic support are shown in Figs. 7 and 8. The friction force is applied simultaneously on the left and right elastic supports, $N_1 = N_2 = 20$ N.

Figure 7 is the mode shape of the rotor with the different stiffness of elastic supports, it is shown that the deflection of the disk increases in comparison to the deflection of the bearings with increase of stiffness. Its means that the smaller the stiffness coefficient of the elastic supports, the more vibration energy is concentrated in the elastic support.

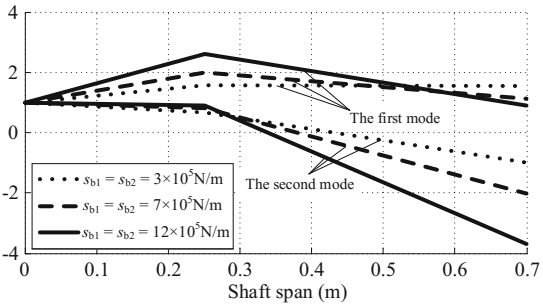

Fig. 7. Mode shape of the rotor

Figure 8 shows the simulation results of the unbalance response of the rotor with the different stiffness of elastic supports. It is shown that the damping performance of the ESDFD is closely related to the operating speed of the rotor and the characteristics of the rotor's mode. Even the same dampers fixed on different rotors or different support locations can perform differently.

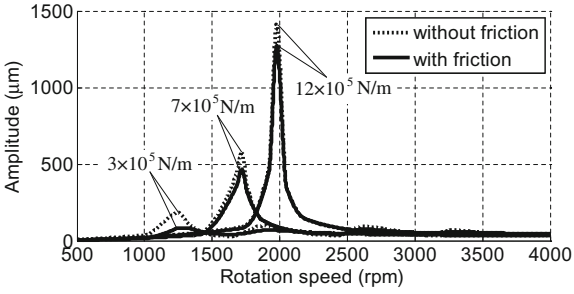

Fig. 8. Unbalance response of the rotor

Pressure Force and the Friction Coefficient

The damping provided by an ESDFD to a rotor is derived from the sliding friction force between the stationary and moving disks. So, as the product of the pressure forces N_1 and N_2 and the friction coefficient μ, the sliding friction forces μN_1 and μN_2 directly determine the damping performance of the damper.

Figure 9 is the simulation results of the unbalance response of the rotor with the different sliding friction forces.

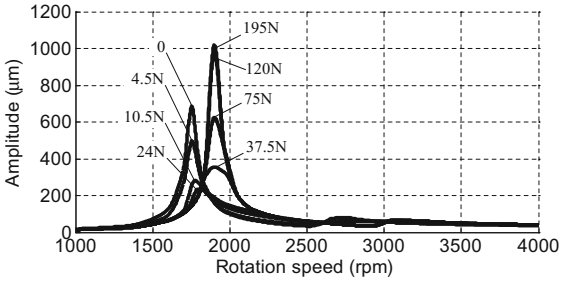

Fig. 9. Unbalance response of the rotor

It is shown in Fig. 9 that as the sliding friction forces μN_1 and μN_2 increase, the critical speed of the rotor system moves upward, and the peak amplitude of the rotor at the critical speed decreases and then increases. When the sliding friction forces are large enough, the peak amplitude of the rotor even exceeds the peak amplitude without friction. There must be an optimal sliding friction force under which the unbalance response of the rotor system will be smallest for all rotational speeds, and the rotor can pass through the critical speed smoothly. In this model, the optimal sliding friction force is between 24 N and 37.5 N.

Stiffness of the Stationary Disk and Tangential Contact Stiffness of the Contact Interface

Between the moving disk and the mounting base of the stationary disk, there is a combined stiffness that consists of the stiffness of the stationary disk and the tangential contact stiffness of the contact interface.

The Stiffness of the Stationary Disk

Figure 10 is the simulation results of the unbalance response of the rotor with the stiffness the stationary disk. The stiffness the stationary disks $s_{j1} = s_{j2,}$ and the pressure forces of the two dampers, applied simultaneously $N_1 = N_2 = 150$ N. It is shown that as the stiffness coefficient of the stationary disk increases, the peak amplitude of the rotor decreases, while the damping performance of the elastic support/dry friction damper improves. When the stiffness coefficients s_{j1} and s_{j2} increase to some extent, the unbalance response curve is nearly constant and the damping performance of the damper no longer changes.

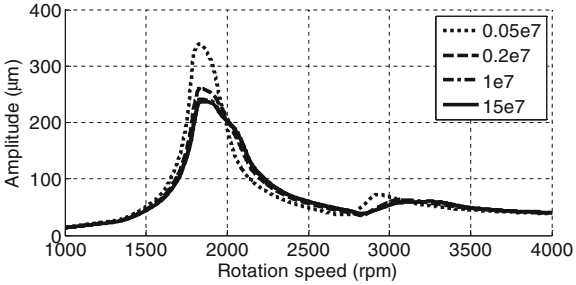

Fig. 10. Unbalance response of the rotor

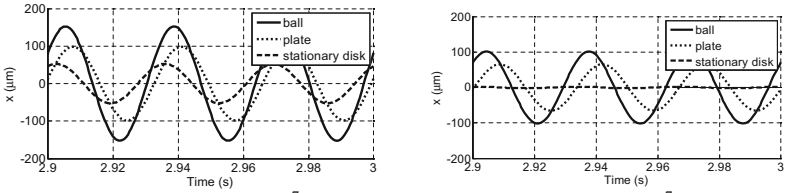

a. $s_{j1} = s_{j2} = 0.05 \times 10^7$ N/m b. $s_{j1} = s_{j2} = 1 \times 10^7$ N/m

Fig. 11. Time domain waveform of the left support

Figure 11 is the simulation results of time domain waveform of the left support at 1800 rpm. As shown in Fig. 11a, when the stiffness coefficient is small, $s_{j1} = s_{j2} = 0.05 \times 10^7$ N/m, the motion of the stationary disk under the traction of the moving disk is obvious, which makes the relative motion between the moving and stationary disks smaller, which is unfavourable for the damping performance of the elastic support/dry friction damper. In Fig. 11b, when the stiffness coefficient is large, $s_{j1} = s_{j2} = 1 \times 10^7$ N/m, the stationary disk barely moves, which is very favorable for the damper.

The Tangential Contact Stiffness of the Contact Interface

Figure 12 is the simulation results of unbalance response of the rotor with the tangential contact stiffness k and the pressure forces of the two dampers, applied simultaneously $N_1 = N_2 = 150$ N. It is shown that as the stiffness coefficient k increases, the peak amplitude of the rotor decreases and the damping performance of the elastic support/dry friction damper improves.

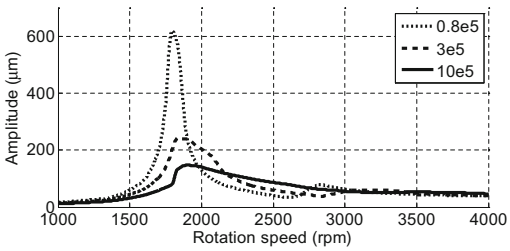

Fig. 12. Unbalance response of the rotor

In the ball/plate model, the plate moves under the traction of the ball. The damping comes from the relative motion between the plate and the stationary disk. When the tangential contact stiffness k is small, the relative motion between the plate and the stationary disk is small, so the damping will be small.

The stiffness of the stationary disk s_j and the tangential contact stiffness of the contact interface k are connected in series between the moving disk and the mounting base of the stationary disk. The larger this combined stiffness is, the better the damper's damping performance.

The Dampers are Applied Different Control Schemes

Due to the additional stiffness of the damper, the critical speed of the rotor system increases as the pressing force increases. This is not allowed for the rotor system. It is necessary to design a control scheme based on the characteristics of the damper, with which that rotor vibration control can be achieved without changing the critical speed of the rotor system. The switch control is one of the most basic control schemes. If the rotational speeds of rotor are within the critical speed regions, the damper is switched on, or the damper switched off. The optimal pressure force N are represented by the control voltage depending simulation results of the damper, or applied proportional (P) control based on the vibration amplitude feedback. The P controller is defined as

$$\mathrm{U} = \mathrm{U}_0 + k_p(PP_D - PP_{D0})$$

Where U is the control voltage, U_0 is the initial voltage, k_p is the proportional gain, PP_D and PP_{D0} are the amplitude of P-P and reference amplitude of P-P, respectively.

The experiments are conducted to investigate the vibration characteristics of the rotor system in switch control scheme. The control voltages are depending on the simulation results and P controller.

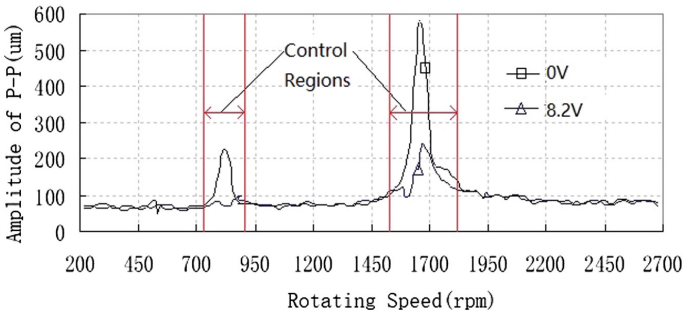

Fig. 13. Diagrams of bode while using switch control at 0 V and 8.2 V

Figure 13 is the amplitude-frequency characteristics of the rotor system at the disk while using switch control and without control in the vertical direction. According to the simulation results, the control voltage is 8.2 V. Comparing to without control, the vibration amplitude of disk is clearly decreased within the critical speed regions, and not changed out of the control regions. At the same time, there is also no change of the critical

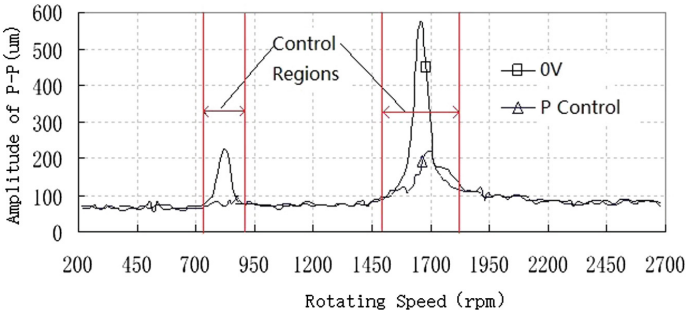

Fig. 14. Diagrams of bode while using switch control at 0 V and P control

speed of the rotor system. The reason is that the additional stiffness of the damper to rotor systems is removed when applied the switch control scheme out of critical regions.

Figure 14 is the amplitude-frequency characteristics of the rotor system at the disk while using switch control and without control in the vertical direction. The control voltages are depending on the P controller. Where U_0 is 3 V, k_p is 0.013, PP_{D0} is 200 μm. Comparing to the control voltage depended on the simulation results, There is the same effect of vibration reduction.

It is shown that switch control scheme is very suitable for the ESDFD to control the vibration of rotor systems actively. It is also possible to optimize vibration control of rotor systems with the ESDFD.

4 Conclusions

Conclusions can be drawn from the theoretical and experimental analysis of the rotor system with the ESDFD:

(1) The ESDFD can effectively control unbalance response of rotor systems around the critical speed by adding the damping and stiffness to rotor systems.
(2) The switch control scheme can effectively controls the ESDFD without changing the critical speed of rotor systems, and the control voltages can be obtained by simulation results or by P controller.
(3) The two-dimensional friction and ball/plate model are very effective in analyzing the steady responses of unbalance. Theoretical results agree with the experimental results to a great extent.

References

1. Fan, T., Liao, M.: Dynamic behavior of a rotor with dry fricition dampers. Mech. Sci. Technol. **22**, 743–745 (2003)
2. Fan, T: Vibration reduction by elastic support dry friction damper. Ph.D. thesis, Northwestern Polytechnical University (2006)

3. Wang, S., Liao, M.: Experimental investigation of an active elastic support/dry friction damper on vibration control of rotor systems. Int. J. Turbo Jet Engines **22**, 13–17 (2014)
4. Wang, S.: Vibration control techniques for rotor systems by an active elastic support/dry friction damper. Ph.D. thesis, Northwestern Polytechnical University (2008)
5. Liao, M., Song, M., Wang, S.: Active elastic support/dry friction damper with piezoelectric ceramic actuator. Shock Vib. ID 712426, 1–10 (2014)
6. Deng, X., Liao, M., Liebich, R., Gasch, R.: Experimental research of bending and torsional vibrations of a double disc rotor due to rotor-to-stator contacts. J. Aerosp. Power **17**, 205–211 (2002)
7. Abu-Mahfouz, I., Banerjee, A.: On the investigation of nonlinear dynamics of a rotor with rub-impact using numerical analysis and evolutionary algorithms. Procedia Comput. Sci. **20**, 140–147 (2013)
8. Oberst, S., Lai, J.C.S., Marburg, S.: Guidelines for numerical vibration and acoustic analysis of disc brake squeal using simple models of brake systems. J. Sound Vib. **332**(9), 2284–2299 (2013)
9. Ma, Y., Zhang, Q., Zhang, D., Scarpa, F., Liu, B., Hong, J.: Tuning the vibration of a rotor with shape memory alloy metal rubber supports. J. Sound Vib. **351**, 1–16 (2015)
10. Griffin, J.H., Menq, C.H.: Friction damping of circular motion and its implications to vibration control. J. Vib. Acoust. **113**, 225–229 (1991)
11. Menq, C.H., Bielak, J., Griffin, J.H.: The influence of microslip on vibratory response, part I: a new microslip model. J. Sound Vib. **107**, 279–293 (1986)
12. Menq, C.H., Griffin, J.H., Bielak, J.: The influence of microslip on vibratory response, part II: a comparison with experimental results. J. Sound Vib. **107**, 295–307 (1986)
13. Ding, Q., Chen, Y.: Analyzing resonant response of a system with dry friction damper using an analytical method. J. Vib. Control **14**(8), 1111–1123 (2008)
14. Liu, C.S., Hong, H.K., Liou, D.Y.: Two-dimensional friction oscillator: group-preserving scheme and handy formulae. J. Sound Vib. **266**, 49–74 (2003)
15. Breard, C., Green, J.S., Vahdati, M., Imregun, M.: A non-linear integrated aero elasticity method for the prediction of turbine forced response with friction dampers. Int. J. Mech. Sci. **43**, 2715–2736 (2001)